University of Reading

Historical tropospheric and stratospheric ozone radiative forcing using the CMIP6 database

Article

Published Version

Creative Commons: Attribution 4.0 (CC-BY)

Open Access

Checa-Garcia, R., Hegglin, M. I., Kinnison, D., Plummer, D. A. and Shine, K. P. (2018) Historical tropospheric and stratospheric ozone radiative forcing using the CMIP6 database. Geophysical Research Letters, 45 (7). pp. 3264-3273. ISSN 00948276 doi: https://doi.org/10.1002/2017GL076770 Available at https://centaur.reading.ac.uk/75867/

It is advisable to refer to the publisher's version if you intend to cite from the work. See Guidance on citing.
Published version at: http://dx.doi.org/10.1002/2017GL076770
To link to this article DOI: http://dx.doi.org/10.1002/2017GL076770

Publisher: American Geophysical Union

All outputs in CentAUR are protected by Intellectual Property Rights law, including copyright law. Copyright and IPR is retained by the creators or other copyright holders. Terms and conditions for use of this material are defined in the End User Agreement.

www.reading.ac.uk/centaur

University of Reading

CentAUR

Central Archive at the University of Reading

Reading's research outputs online

AGU PUBLICATIONS

Geophysical Research Letters

RESEARCH LETTER
10.1002/2017GL076770

Key Points:
- The 1850-2010 ozone radiative forcing for the CMIP6 ozone database is 80% higher than for CMIP5
- The long-term stratospheric ozone radiative forcing in the Northern Hemisphere is positive despite recent ozone depletion
- Tropospheric and stratospheric ozone changes both lead to long-term marked cooling patterns in the stratosphere

Supporting Information:
- Supporting Information S1

Correspondence to:
R. Checa-Garcia,
r.checa-garcia@reading.ac.uk

Citation:
Checa-Garcia, R., Hegglin, M. I., Kinnison, D., Plummer, D. A., & Shine, K. P. (2018). Historical tropospheric and stratospheric ozone radiative forcing using the CMIP6 database. *Geophysical Research Letters*, *45*, 3264–3273. https://doi.org/10.1002/2017GL076770

Received 5 JAN 2018
Accepted 23 FEB 2018
Accepted article online 28 FEB 2018
Published online 6 APR 2018

The copyright line for this article was changed on 23 APR 2018 after original online publication.

©2018. American Geophysical Union. All Rights Reserved.

Historical Tropospheric and Stratospheric Ozone Radiative Forcing Using the CMIP6 Database

Ramiro Checa-Garcia[1], Michaela I. Hegglin[1], Douglas Kinnison[2], David A. Plummer[3], and Keith P. Shine[1]

[1]Department of Meteorology, University of Reading, Reading, United Kingdom, [2]National Center for Atmospheric Research, Boulder, CO, USA, [3]Environment and Climate Change Canada, Montréal, Quebec, Canada

Abstract We calculate ozone radiative forcing (RF) and stratospheric temperature adjustments for the period 1850–2014 using the newly available Coupled Model Intercomparison Project phase 6 (CMIP6) ozone data set. The CMIP6 total ozone RF (1850s to 2000s) is 0.28 ± 0.17 W m^{-2} (which is 80% higher than our CMIP5 estimation), and 0.30 ± 0.17 W m^{-2} out to the present day (2014). The total ozone RF grows rapidly until the 1970s, slows toward the 2000s, and shows a renewed growth thereafter. Since the 1990s the shortwave RF exceeds the longwave RF. Global stratospheric ozone RF is positive between 1930 and 1970 and then turns negative but remains positive in the Northern Hemisphere throughout. Derived stratospheric temperature changes show a localized cooling in the subtropical lower stratosphere due to tropospheric ozone increases and cooling in the upper stratosphere due to ozone depletion by more than 1 K already prior to the satellite era (1980) and by more than 2 K out to the present day (2014).

Plain Language Summary Radiative forcing is a key concept used in climate science to ascertain the strength of different agents, such as greenhouse gases or aerosols among others, in driving climate change. In this context, ozone is recognized as one of the main contributors to radiative forcing according to recent assessments of the Intergovernmental Panel on Climate Change. However, the relative uncertainty remains higher than for other greenhouse gases. This paper evaluates the ozone radiative forcing via calculations based on a newly created ozone data set for the Coupled Model Intercomparison Project (CMIP) phase 6, an initiative designed to better understand past, present, and future climate changes. In general, human activity has led to an increase in ozone concentrations in the lower atmosphere (the troposphere) and decreases in the upper atmosphere (the stratosphere); our paper investigates the effect of both these changes. Our results indicate that the CMIP ozone radiative forcing is 80% larger in the current phase 6 than a similar estimation based on data used in CMIP phase 5. We also present new insights into how ozone changes have led to stratospheric temperature changes, as well as the geographical distribution of ozone radiative forcing.

1. Introduction

The radiative forcing (RF) due to changes in tropospheric and stratospheric ozone is the third largest greenhouse gas contributor to RF since preindustrial (PI) times (Myhre et al., 2013). However, ozone's RF has a much higher relative uncertainty than the well-mixed greenhouse gases. For the well-mixed greenhouse gases, which are characterized by long lifetimes and relatively homogeneous distributions, surface observations from a rather few sites provide reasonable constraints on global trends in gas concentrations: observations from firn ice and ice cores allow these data records to be extended to periods before in situ observations began. By contrast, the horizontal and vertical inhomogeneity in ozone makes it more difficult to observe and characterize its distribution and trends, even for recent times. These difficulties become progressively larger further back in time, and there is little information, except for a few surface sites in the last nineteenth century (Cooper et al., 2014). Hence, estimates of ozone RF rely heavily on models that aim to simulate the evolution of the ozone. There are added difficulties in that both longwave (LW) and shortwave (SW) radiation contribute significantly to the total ozone forcing (and can even be of opposing sign, in the case of stratospheric forcing), whereas for well-mixed greenhouse gases the LW is normally the dominant term. In addition, at least since the middle of the twentieth century, ozone has been increasing in the troposphere

and decreasing in the stratosphere, due to the combined effects of air pollutants and ozone depleting substances, making the net forcing a residual of opposing terms.

Advances in chemical modeling of the atmosphere have improved our understanding of the drivers of ozone change, and multimodel comparisons have allowed estimates of the uncertainties in the role of these drivers (e.g., Young et al., 2013). The Stratosphere-troposphere processes And their Role in Climate/Atmospheric Chemistry and Climate (SPARC/ACC) ozone data set prepared for the Coupled Model Intercomparison Project phase 5 (CMIP5) (Cionni et al., 2011) used climate models with interactive chemistry to represent the evolution of tropospheric ozone and zonal-mean data based on available observations for the stratosphere. The more recent International Global Atmospheric Chemistry (IGAC)/SPARC Chemistry-Climate Model Initiative (CCMI) ozone data set, designed for CMIP6, instead uses models which span the troposphere and middle atmosphere in a fully interactive way (Morgenstern et al., 2017), therefore providing consistent ozone fields in time and space. In consequence, it is expected that the improvements in the latest generation of chemistry-climate models will impact the calculations of ozone's RF.

This paper calculates the RF of ozone, from the new CMIP6 data set; using the same methodology, we also calculate RF from the CMIP5 data set to allow for a consistent comparison. We calculate the RF separately for changes in tropospheric and stratospheric ozone for each decade in the period 1850–2014, and the change in stratospheric temperature by using the fixed dynamical heating (FDH) approach. We assess the main characteristics of the resulting RF derived using CMIP6 data. The data used in our study are described in section 2, the methodology in section 3, and results in section 4, followed by a concluding discussion in section 5.

2. Data

The estimation of the RF for a specific agent needs the definition of a background and a perturbed state (PS) of that agent. Here we define the PI background state as monthly means for the 1850–1859 decade. We then perform RF calculations for monthly means for each decade from 1860–1869 to 2000–2009 and for 2010–2014 (the most recent historical period in the CMIP6 data base). We refer to them as the perturbed state. This approach is similar to the analysis of CMIP5 data by Cionni et al. (2011).

We use the original CMIP5 (Cionni et al., 2011) and the new CMIP6 ozone concentration data sets as three-dimensional fields interpolated onto a grid of $3^\circ \times 3^\circ$ horizontal resolution and the L60 σ-p model levels of ERA-Interim. The climatology of nonozone components (temperature, humidity, albedo, and cloud parameters) is obtained from monthly means of the ERA-Interim reanalysis (Dee et al., 2011) averaged over the time period 2000–2009. The main greenhouse gas concentrations CO_2, CH_4, and N_2O, as well as chlorofluorocarbons (CFCs) and hydrochlorofluorocarbons (HCFCs), are included in the radiative transfer scheme, at the PI values for 1850, taken from Intergovernmental Panel on Climate Change (IPCC) Fifth Assessment Report (AR5) (Myhre et al., 2013). The cloud parameters used in the off-line radiative transfer scheme differentiate ice and liquid water clouds which are modeled with the European Centre for Medium-Range Weather Forecasts (ECMWF) ReAnalysis, ERA-Interim vertically resolved liquid and ice water contents. From the total cloud fraction we estimate the liquid and ice cloud fraction, and we consider an aerosol-free atmosphere as in other recent studies of ozone RF (e.g., Rap et al., 2015); see supporting information for details.

3. Methods

The RF is estimated with the off-line radiative transfer model included in the Suite of Community Radiative Transfer codes based on Edward and Slingo (SOCRATES), e.g. Edward and Slingo (1996), which estimates the radiative fluxes with a two-stream scheme. In the main model setup used in this paper, the model has six broadbands in the SW and nine broadbands in the LW. SOCRATES has been extended to compute RF (named SOCRATES-RF here) by calculating the stratospherically adjusted temperatures as described in Forster et al. (1997). A similar method to estimate the RF, also based on Edwards and Slingo (1996), was previously used for the CMIP5 and Atmospheric Chemistry and Climate Model Intercomparison Project (ACCMIP) estimations (Cionni et al., 2011; Stevenson et al., 2013). The methodology follows the definition used by Ramaswamy, Boucher, et al. (2001) where the change in irradiance is evaluated when stratospheric temperatures are readjusted assuming the standard FDH approach, performed separately for each month. The method requires the definition of a tropopause to specify the region above which temperatures are adjusted. Cionni et al. (2011) used a tropopause based on the 2 potential vorticity unit (PVU) definition and the NCEP/NCAR reanalysis. Stevenson et al. (2013) also compared the use of tropopauses based on a specific ozone threshold

(e.g., Young et al., 2013) or change in the temperature gradient (e.g., Myhre & Stordal, 1997), and found that the tropopause choice had only a marginal impact on RF values. In our study we modeled the climatological tropopause defined by Hansen et al. (2005) with a parametric equation described in the supporting information (section S2).

Our methodology includes stratospheric temperature adjustments but not rapid tropospheric adjustments. Both are required to estimate the effective radiative forcing (ERF), which is regarded as being more directly related to surface temperature change (Myhre et al., 2013). Because ERFs require climate models for their calculation, they are inherently noisy, due to the internal variability generated by them, and can be difficult to detect, particularly for the small ozone forcings earlier in our 1850–2014 period. Shindell et al. (2013) show that the global-mean ERFs are, within their uncertainties, generally consistent with the RFs calculated using the method we use here, and Myhre et al. (2013) concluded that differences between RF and ERF for ozone change are likely to be small. However, Shindell et al. (2013, Figure 25) show a stronger latitudinal variation in the southern hemisphere (SH) for the ozone ERF than RF, at least for their model, so more caution may be needed in interpreting the geographical patterns of RF presented here.

Further, our separation of tropospheric and stratospheric ozone RF is based on a (latitudinally varying) tropopause pressure. An alternative framework (e.g., Shindell et al., 2013, Søvde et al., 2011, 2012) separates forcings via the driver of the ozone change, for example, ozone depleting substances and tropospheric ozone precursors. Since ozone depleting substances influence tropospheric ozone and tropospheric ozone precursors influence stratospheric ozone, via direct chemical impacts and changes in stratosphere-troposphere exchange, this framework would produce a different division of forcings than the one we present. CMIP6 ozone data do not currently offer the information to use that framework.

4. Results

4.1. Global Estimates of Ozone RF

We investigate first the global-mean tropospheric and stratospheric ozone RF using CMIP6 and compare it with CMIP5 calculations for the 2000s decade (Table 1). The tropospheric ozone RF is 40% larger using CMIP6 instead of CMIP5: 0.31 W m^{-2} versus 0.22 W m^{-2} (this latter value is consistent with the Cionni et al., 2011, estimate of 0.23 W m^{-2} using CMIP5). The stratospheric ozone RF using CMIP6 is −0.033 W m^{-2}, compared to −0.073 W m^{-2} using CMIP5. The total ozone RF is 80% greater using CMIP6 ozone: 0.28 W m^{-2} compared to 0.15 W m^{-2} using CMIP5 (which is almost identical to the Cionni et al., 2011, CMIP5 estimate of 0.151 W m^{-2}). Despite the significant changes with respect to CMIP5, the new estimate using CMIP6 ozone is more consistent with IPCC-AR5 central values (0.36 and −0.05 W m^{-2} for tropospheric and stratospheric ozone RF respectively as shown in Figure 1 which, for consistency, exclude the 1750–1850 contribution to RF) than using CMIP5 ozone.

The right-hand column of Figure 1 shows the time evolution of CMIP6-RF (including the individual LW and SW components) together with the IPCC-AR5 values (Myhre et al., 2013). There is a continuous increase in the tropospheric ozone RF which accelerated in the 1960s and slowed after the 1980s; our CMIP6 calculation tracks below the AR5 value but with similar shape; as is expected from earlier work the main contribution is from the LW (e.g., Cionni et al., 2011). This time dependence is consistent with CMIP6 global tropospheric ozone column (Figure 1, left column, first panel), which shows a systematic increase until the 1980s, primarily due to the northern hemisphere (NH) contribution with a slight hiatus in recent decades due to a decrease in SH tropospheric ozone.

The net stratospheric ozone RF is close to zero until the 1950s at which it turns slightly positive for two decades and then turns negative primarily due to the strong SH ozone depletion, consistent with the evolution of the stratospheric ozone burden also shown in Figure 1. It also shows a comparison of the CMIP6 ozone total column with that from Multisensor Reanalysis version 1 (van der A et al., 2010) in the satellite era, demonstrating good agreement within the Multisensor Reanalysis uncertainties and consistency in the trends. Notably, both the SW and LW RF switch signs between the 1960s and the post-1980 period, with the net RF being a small residual of the two and with an increasing divergence until 2014. The IPCC-AR5 stratospheric ozone RF remains negative throughout, but the CMIP6-RF is consistent with the positive RF due to the effect of tropospheric ozone precursors (including NO_x and methane) on stratospheric ozone since 1990 (Søvde et al., 2011, 2012). The small perturbation in stratospheric ozone RF in the 1880s is likely a transient dynamical response of ozone to volcanic aerosol loading in this period, which is included in the CMIP6 forcing data set.

Table 1
Estimates of All-Sky Ozone RF Based On the CMIP5 and CMIP6 Ozone Data Sets Relative to 1850–1859 for Tropospheric, Stratospheric, and Total Ozone Changes and for LW, SW, and Net Components Shown for Each Case

		Tropospheric (W m^{-2})			Stratospheric (W m^{-2})			Total (W m^{-2})		
Region	PS/PI	SW	LW	Net	SW	LW	Net	SW	LW	Net
Global	CMIP6-2000s/CMIP6	0.070	0.242	0.312	0.095	−0.128	−0.033	0.165	0.114	0.279
Global	CMIP5-2000s/CMIP5	0.047	0.178	0.225	0.175	−0.247	−0.073	0.222	−0.069	0.153
Global	CMIP6-2000s/CMIP5	0.071	0.266	0.337	0.215	−0.267	−0.051	0.286	−0.001	0.285
Global	CMIP5-2000s/CMIP6	0.046	0.154	0.199	0.054	−0.107	−0.053	0.100	0.047	0.146
Global	Cionni et al. (2011)	0.084	0.146	0.229	0.122	−0.200	−0.078	0.206	−0.054	0.151
Global	Stevenson et al. (2013)	0.060	0.255	0.315	-	-	-	-	-	-
Global	CMIP6-2010s/CMIP6	0.074	0.255	0.329	0.080	−0.109	−0.029	0.154	0.146	0.300
NH	CMIP6-1970s/CMIP6	0.077	0.235	0.312	−0.007	0.035	0.027	0.070	0.270	0.339
NH	CMIP6-2000s/CMIP6	0.110	0.341	0.451	0.060	−0.027	0.034	0.170	0.314	0.485
NH	CMIP6-2010s/CMIP6	0.116	0.360	0.476	0.043	−0.002	0.041	0.159	0.358	0.517
SH	CMIP6-1970s/CMIP6	0.034	0.127	0.161	0.021	−0.034	−0.013	0.054	0.093	0.158
SH	CMIP6-2000s/CMIP6	0.029	0.143	0.172	0.133	−0.232	−0.099	0.162	−0.089	0.071
SH	CMIP6-2010s/CMIP6	0.031	0.150	0.181	0.121	−0.220	−0.099	0.152	−0.070	0.082

Note. Note that clear-sky values are shown in Table S6, while values of RF for all decades are shown in Tables S11 and S12 in the supporting information. The 5–95% uncertainty is considered to be ±0.5 times the central estimated value for tropospheric ozone and ±2 times for stratospheric ozone radiative forcing (RF) (see, e.g., Myhre et al., 2013). CMIP5 = Coupled Model Intercomparison Project phase 5; CMIP6 = Coupled Model Intercomparison Project phase 6; LW = longwave; SW = shortwave; NH = northern hemisphere; SH = southern hemisphere. PS = Perturbed State; PI = Pre-Industrial state.

When both stratospheric and tropospheric RF are combined (Figure 1, last row) the net RF shows a notable slowdown after about 1980. Checa-Garcia et al. (2016) calculated that the slowdown in the growth in tropospheric ozone RF contributed 5–11% to the observed slowdown in surface temperature increases, also referred to as a hiatus in global warming. Between 1920 and 1980, the CMIP6 RF is very close to the IPCC-AR5 values. Another notable feature is the change in relative importance of the LW and SW components over recent decades, with the SW forcing dominating over the LW forcing in the most recent two decades, as a result of the rapid changes in stratospheric ozone RF (and its LW and SW components). Shindell et al. (2013) found a similar result in their instantaneous RF calculations; our results confirm that the feature is present when stratospheric temperature adjustment is included.

The ozone changes also induce changes on the stratospheric temperature due to changes in both reflected SW radiation and upwelling LW radiation from the troposphere. We estimate the temperature changes (ΔT) using the FDH approach for both tropospheric and stratospheric ozone change. While dynamical responses would be expected to modify the FDH-derived changes, FDH provides a good first-order estimate. The impact of stratospheric ozone depletion on stratospheric temperature changes is well recognized (e.g., Ramaswamy, Chanin, et al., 2001; Seidel et al., 2011), but comparatively little attention has been given to the role of tropospheric ozone change (see, e.g., Berntsen et al., 1997; Ramaswamy & Bowen, 1994; Sexton et al., 2003). Figure 2 shows the derived ΔT for the tropospheric and stratospheric ozone perturbations separately, and for both (estimated here as the sum of the individual effects), for each decade since the 1970s, all relative to the 1850s. First, we note cooling in the lower stratosphere due to the tropospheric ozone increases which is most marked in the subtropics (25°N and 25°S); this is clearest in the NH where temperatures decreases by more than 1.4 K in the 2000s, but it is also found in the SH with a cooling of 0.8 K. These patterns have grown continuously since the 1970s, with the area of largest cooling in the NH progressively extending deeper into the stratosphere. The latitudinal pattern of the ΔT is similar to that in Berntsen et al. (1997) but more intense. It matches the geographical pattern of the forcing (see section 4.4), which peaks in the subtropics (and in particular in the NH) and hence causes the largest decrease in the absorption of upwelling irradiance in the lower stratosphere.

We now focus on the ΔT due to stratospheric ozone change (middle row of Figure 2). The general pattern of ΔT for the recent period is generally understood (e.g., Shine et al., 2003) with maximum cooling in the upper stratosphere, a relative minima (and even a slight warming) in the midstratosphere, and a secondary

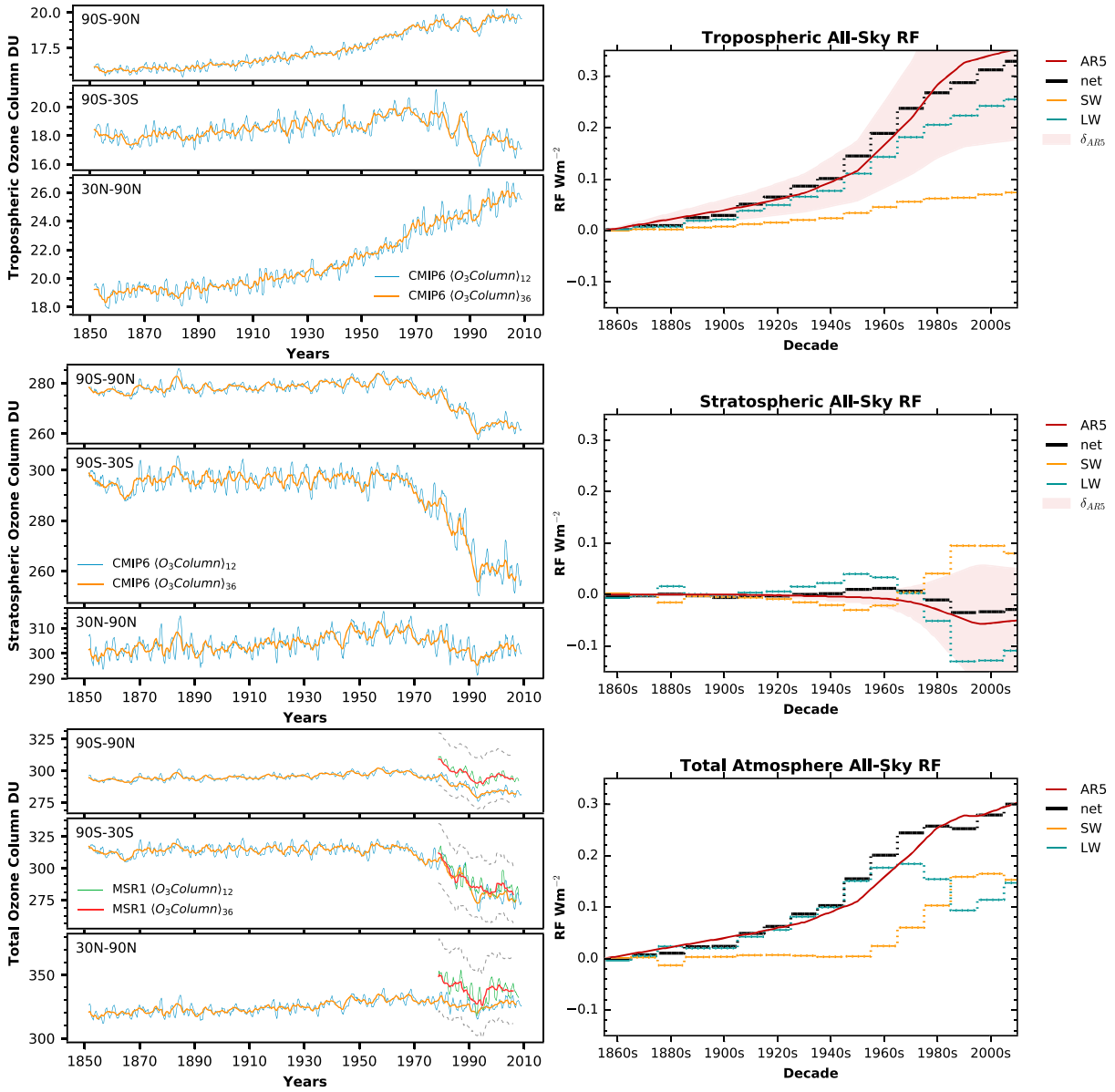

Figure 1. Ozone column (in Dobson Units, DU) and global values of stratospherically adjusted radiative forcing (RF) (W m^{-2}) relative to the 1850–1859 decade for the CMIP6 ozone data set. Left column: 12 (blue) and 36 months (orange) moving average time series of ozone column for the troposphere, stratosphere, and total column and three different latitudinal bands. For the total ozone column the Multisensor Reanalysis version 1 reanalysis data set (van der A et al., 2010) is shown in green/red (12/36 months moving average) and its uncertainty range with grey dashed lines. Right column: radiative forcing due to troposphere, stratosphere, and total atmosphere ozone changes. The red lines are RF values from IPCC-AR5 with respect to 1850s (with uncertainty shaded in red); the stepped line is our decadal-mean estimate for shortwave (SW) (orange), longwave (LW) (blue), and net forcing (black). Note that the IPCC-AR5 time series is drawn such that the 1860s tickmark corresponds to the year 1865.

maximum in the lower stratosphere, which is particularly marked in high southern latitudes, associated with the ozone hole. Most recent work has concentrated on temperature changes since the late 1970s, for which more observations are available. However, Figure 2 shows that the calculated cooling in the upper stratosphere had already exceeded 1 K during the 1970s, and it is only by the 1990s that the cooling in the Antarctic lower stratosphere exceeds the upper stratospheric cooling. For the most recent decade, the cooling exceeds 2.5 K in much of the upper stratosphere and 5 K in the Antarctic lower stratosphere. Part of the warming in the lower and midstratosphere, particularly in the 1970s in the NH, is likely driven by the increase in stratospheric ozone as a result of the tropospheric ozone precursors discussed above. The ΔT due to stratospheric ozone after 1980 is consistent with earlier work (e.g., Jonsson et al., 2009; Seidel et al., 2011; Shine et al., 2003)

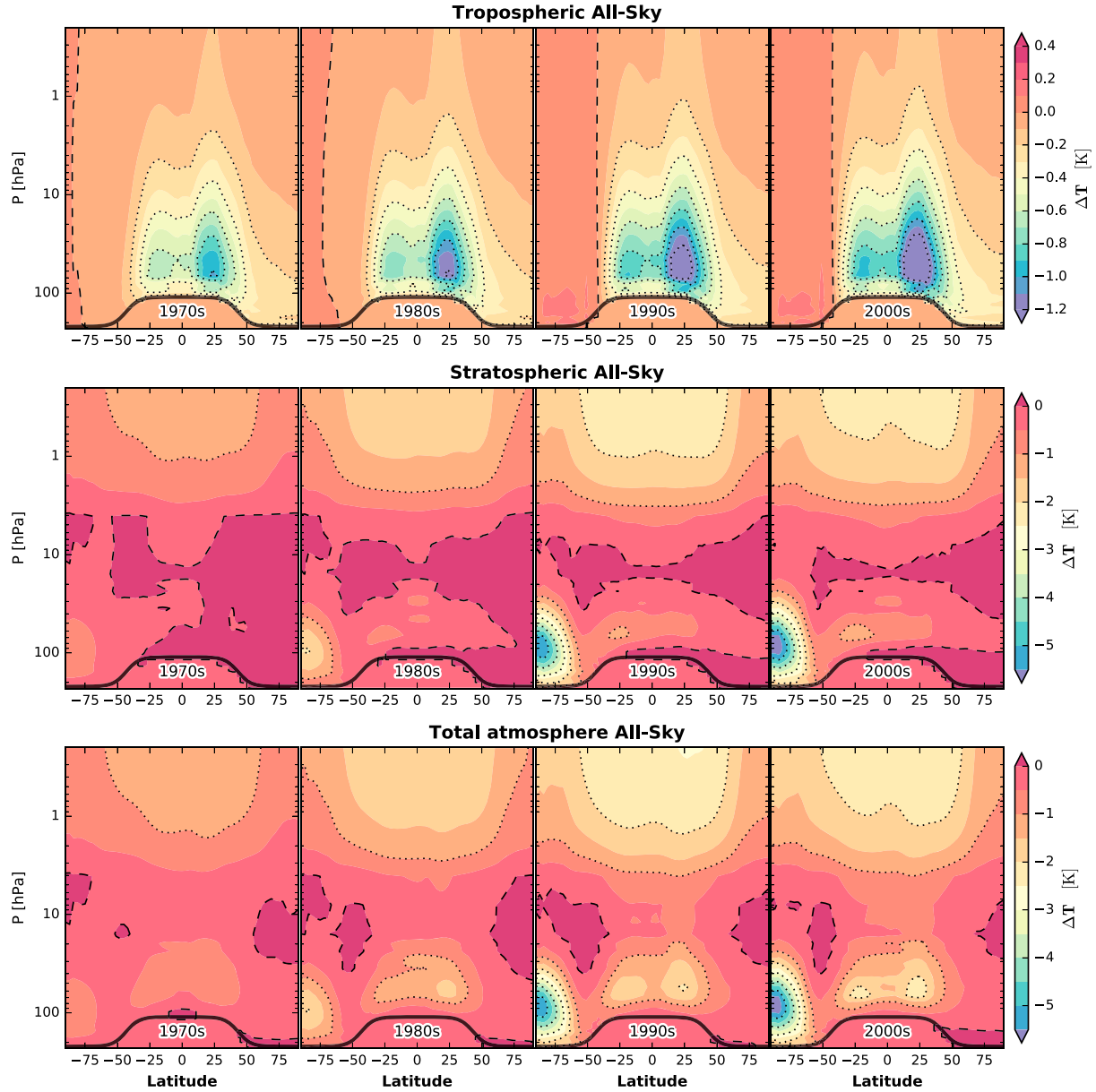

Figure 2. Changes in stratospheric temperatures (ΔT in K) due to changes in Coupled Model Intercomparison Project phase 6 ozone concentrations calculated using the fixed dynamical heating approach. For tropospheric (top row), stratospheric (middle row), and total ozone changes (bottom row) for the four decades from 1970 to 2000s relative to the 1850s.

both in magnitude and vertical structure. The CO_2-induced cooling both in recent decades (Jonsson et al., 2009) and since PI times (Schwarzkopf & Ramaswamy, 2008) is similar to that due to ozone, while in the lower stratosphere the ozone-induced cooling dominates over CO_2 in recent decades (e.g., Seidel et al., 2011). The combined CO_2 and ozone temperature trends in the upper stratosphere is consistent with satellite-derived trends since 1980 (e.g., McLandress et al., 2015; Seidel et al., 2011); consistency between model and observed trends in the lower stratosphere remains dependent on assumptions about trends in stratospheric water vapor (Seidel et al., 2011).

The bottom row of Figure 2 shows the ΔT due to both tropospheric and stratospheric ozone change. While the overall pattern is dominated by the effect of stratospheric ozone change, the signature of the cooling due to the tropospheric ozone increases is still visible in the lower stratosphere in the subtropics, close to 2.5 K in the 2000s. This pattern has been accentuated in recent decades.

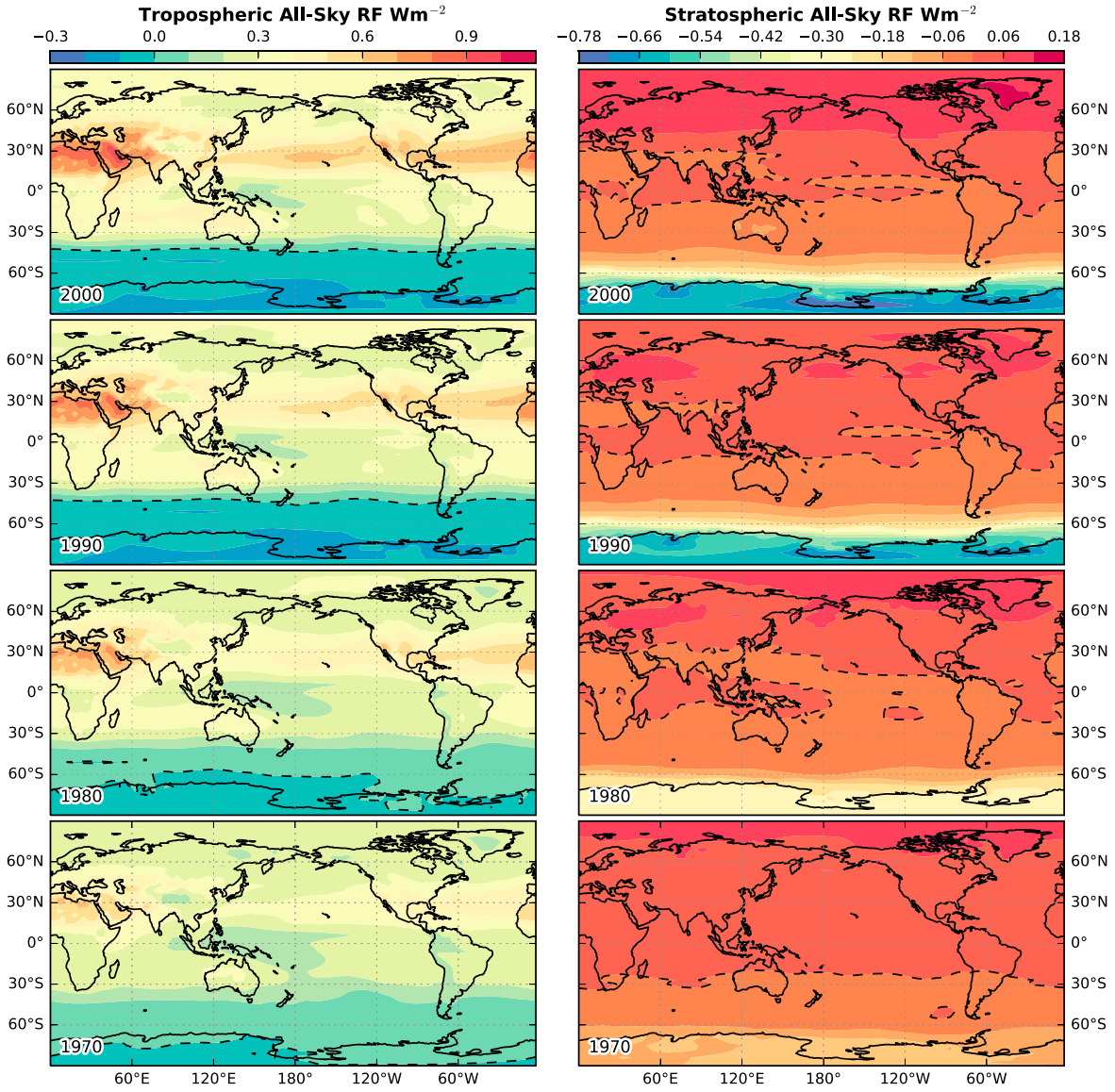

Figure 3. Geographical distribution of radiative forcing (W m^{-2}). (left column) Radiative forcing (RF) due to tropospheric ozone changes for the decades 2000s, 1990s, 1980s, and 1970s (all with respect to 1850–1859). (right column) Same as the left column but for the stratospheric ozone change.

4.2. Uncertainties in Global Mean

Previous studies indicate that a major source of uncertainty in the ozone RF is the PI ozone concentrations (Stevenson et al., 2013). To further understand this, two additional estimates of RF have been calculated where the PS/PI concentrations considered are CMIP6/CMIP5 and CMIP5/CMIP6 (see Table 1). The use of CMIP6-PS state with CMIP5-PI increases tropospheric RF by 8%, while the stratospheric RF is more negative by more than 50% which leads to a net RF similar to the CMIP6/CMIP6 case. However, the values of LW and SW RF for the stratospheric ozone case are markedly different, which is most likely due to the use of a limited multiple linear regression to infer the CMIP5-PI stratospheric ozone distribution instead of a fully coupled model. The use of CMIP5/CMIP6 case leads to a decrease of tropospheric ozone RF by 12% relative to CMIP5/CMIP5. The stratospheric ozone RF is close to CMIP6/CMIP5 but with a markedly different LW/SW contributions showing that they are severely affected by the PI concentrations. The difference between the CMIP6 and CMIP5 PI values is a source of significant uncertainty, but more so in partitioning of the forcing between stratospheric and tropospheric ozone RF and between the LW and SW components than in the final total net RF. Nevertheless, these calculations emphasize that most of the difference in the CMIP6 and CMIP5 ozone RFs arises from the change in ozone since PI times, rather than from the PI values themselves.

We considered further uncertainty sources. Changes in the tropopause specification and in the spectral file used by SOCRATES-RF have only a marginal impact on the forcing, as does degrading the horizontal resolution from 3×3 to $5 \times 5°$. Sensitivity studies using different assumptions for the tropopause, spectral data and grid resolution are shown in the SI (Tables S8–S10, respectively).

An important uncertainty in the ozone RF remains the choice of models to create the ozone database itself due to different sensitivities to emissions, climate forcers, and chemistry-climate feedbacks. To account for this uncertainty, we retain the uncertainty given by IPCC-AR5 for tropospheric and stratospheric ozone (as described in Table 1). The total ozone RF uncertainty assumes that these uncertainties are uncorrelated.

4.3. Seasonal Cycle

There is a strong seasonal cycle in both tropospheric and stratospheric ozone RF (bottom row of Figure S1 in the supporting information). This is primarily due to the seasonal variations of ozone changes, with the largest perturbations being in NH summer in the troposphere and SH spring in the stratosphere. The strong seasonal cycle in stratospheric ozone RF emerged only in recent decades due to the Antarctic ozone hole. For tropospheric ozone RF, the peak forcing in the summer months has become increasingly accentuated in recent decades (see Figure S1), this is consistent with the behavior reported in Rap et al. (2015) for the global mean radiative effect based on remote sensing of ozone concentrations that shows a maximum in tropospheric ozone RF in NH summer months and a minimum in NH winter.

4.4. Spatial Distribution

A notable result is the different hemispheric contributions to the global-mean RF. As expected from many previous studies (e.g., Berntsen et al., 1997; Cionni et al., 2011; Rap et al., 2015; Shindell et al., 2013), the NH ozone forcing exceeds the SH value. NH mean values for the 1970s, 2000s, and 2010s decades increase in time (Table 1) and illustrate the stronger contribution of NH to ozone RF in the net RF which is 5 times larger for the NH than SH in the 2010s. This also results in the NH trospospheric ozone RF being more than 2 times the SH value due to its higher ozone precursor emissions, plus the impact of a Antarctic stratospheric ozone depletion on SH ozone concentrations. These results are consistent with the first row of Figure S1 in the supporting information, which shows increasing differences between NH and SH RF values which become more marked since the 1970s.

Figure 3 gives additional insight on the evolution of the geographical distribution of RF. The overall pattern is generally consistent with previous work (e.g., the higher forcing in NH subtropics, with a peak over the dry zones, which results from a combination of large changes in tropospheric ozone and high values of outgoing LW radiation, e.g., Berntsen et al., 1997, due to the combination of higher surface temperatures and cloud-free skies). The negative tropospheric ozone RF in the SH extratropics is similar to but more intense than that found by Cionni et al. (2011) using CMIP5 ozone, and in contrast to that work, the stratospheric ozone RF is positive everywhere outside the SH extratropics in the 1970s and remains positive in the NH during the 2000s (see Table 1).

5. Discussion and Conclusions

We have calculated the RF using the newly available CMIP6 historical ozone forcing data set. For the period 1850–2010 the total ozone RF is found to be 80% higher than the CMIP5 ozone RF, with the same radiation scheme and meteorological fields. This results from an increased tropospheric ozone RF of 40%, and a stratospheric ozone RF which is about 60% less negative. The ozone RF using CMIP6 is closer to the midrange values provided by IPCC-AR5 report. The present-day (2000–2014 relative to 1850–1860) RF is 0.33 W m^{-2} for tropospheric ozone, −0.029 W m^{-2} for stratospheric ozone, yielding a total ozone RF of 0.30 W m^{-2}. The 5–95% confidence interval is given by 0.16 to 0.49 W m^{-2} and −0.087 to 0.029 W m^{-2} for tropospheric and stratospheric RF, respectively.

In marked contrast to CMIP5 and IPCC-AR5, prior to the 1970s, the stratospheric ozone RF was positive before turning negative. This time, variation likely reflects competition between the effects of precursors (which are traditionally regarded as *tropospheric*) and ODS. The mean NH stratospheric ozone RF remains positive throughout the 1850–2014 period; the more recent ozone loss does not compensate for the preceding, longer-term increase. Accompanying these trends are marked changes in the individual LW and SW components. Prior to the 1970s, SW forcing is negative, switching to positive after 1970; the LW forcing mirrors these changes. The time evolution of the tropospheric ozone RF since 1850 is very similar to IPCC-AR5 until the 1980s

but shows a more marked slowdown in the growth since then. As expected, the LW forcing is the dominant component throughout.

The time evolution of the total ozone RF is similar to IPCC-AR5 up until the 1940s. After that and until the end of the 1960s, it is more positive, partly because of the positive stratospheric ozone RF during this period. Since the 1970s, it has grown, on average, more slowly, due to the combined effect of the slower growth in the tropospheric ozone RF and the stratospheric ozone RF turning negative. A striking feature is that prior to the 1980s, the LW forcing was the larger component but, mostly driven by the effect of stratospheric ozone depletion, the SW forcing exceeded the LW component until the 2010–2014 period when the LW and SW are approximately equal.

The stratospheric temperature adjustment was estimated using the FDH method. The cooling due to stratospheric ozone shows characteristic peaks in the lower and upper stratosphere (with the lower stratosphere cooling most marked in the Antarctic), with a slight midstratosphere warming at most latitudes. However, our calculations show that upper stratospheric cooling prior to the satellite period had already exceeded 1 K by the 1970s, and so giving a total cooling exceeding 2 K up to the present day. They also show that tropospheric ozone increases have led to a marked cooling of the lower stratosphere, peaking in the subtropics, associated with regions of high outgoing long-wave radiation (which are hence more sensitive to ozone change). The cooling influence of tropospheric ozone has been much less recognized in the literature. By 2000–2010, the NH cooling due to tropospheric ozone increases exceeds 1 K, with an influence that extends through the midstratosphere. This significantly modifies the pattern due to stratospheric ozone depletion alone, not only in the tropical lower stratosphere but also in the midstratosphere, where the band of warming is no longer found.

Acknowledgments
The authors acknowledge the support of UK Natural Environment Research Council research grant SMURPHS (NE/N006054/1) led by Piers Forster at the University of Leeds. We acknowledge the WCRP IGAC/SPARC Chemistry-Climate Model Initiative (CCMI) for coordination of the activity and the involved modeling groups for the generation of additional model simulations that were needed to produce this ozone database in support of CMIP6 (the database is accessible via the input4MIPs data server; more information is given in the supporting information). James Manners at the UK Met Office is thanked for making the original SOCRATES radiative transfer code available. Douglas Kinnison would like to acknowledge the support of the National Center for Atmospheric Research (NCAR), supported by the U.S. National Science Foundation (NSF) and Climate Simulation Laboratory (CISL). David Plummer would like to thank the Canadian Foundation for Climate and Atmospheric Sciences and the Canadian Space Agency for supporting the development of CMAM. We also thank two reviewers for their helpful comments.

References

Berntsen, T. K., Isaksen, I. S. A., Myhre, G., Fuglestvedt, J. S., Stordal, F., Larsen, T. A., et al. (1997). Effects of anthropogenic emissions on tropospheric ozone and its radiative forcing. *Journal of Geophysical Research*, *102*(D23), 28,101–28,126. https://doi.org/10.1029/97jd02226

Checa-Garcia, R., Shine, K. P., & Hegglin, M. I. (2016). The contribution of greenhouse gases to the recent slowdown in global-mean temperature trends. *Environmental Research Letters*, *11*(9), 94018. https://doi.org/10.1088/1748-9326/11/9/094018

Cionni, I., Eyring, V., Lamarque, J. F., Randel, W. J., Stevenson, D. S., Wu, F., et al. (2011). Ozone database in support of CMIP5 simulations: Results and corresponding radiative forcing. *Atmospheric Chemistry and Physics*, *11*(21), 11,267–11,292. https://doi.org/10.5194/acp-11-11267-2011

Cooper, O. R., Parrish, D. D., Ziemke, J., Balashov, N. V., Cupeiro, M., Galbally, I. E., et al. (2014). Global distribution and trends of tropospheric ozone: An observation-based review. *Elementa: Science of the Anthropocene*, *2*, 29. https://doi.org/10.12952/journal.elementa.000029

Dee, D. P., Uppala, S. M., Simmons, A. J., Berrisford, P., Poli, P., Kobayashi, S., et al. (2011). The ERA-Interim reanalysis: Configuration and performance of the data assimilation system. *Quarterly Journal of the Royal Meteorological Society*, *137*(656), 553–597. https://doi.org/10.1002/qj.828

Edwards, J., & Slingo, A. (1996). Studies with a flexible new radiation code. I: Choosing a configuration for a large-scale model. *Quarterly Journal of the Royal Meteorological Society*, *122*(531), 689–719. https://doi.org/10.1002/qj.49712253107

Forster, P. M., Freckleton, R. S., & Shine, K. P. (1997). On aspects of the concept of radiative forcing. *Climate Dynamics*, *13*(7), 547–560. https://doi.org/10.1007/s003820050182

Hansen, J., Sato, M., Ruedy, R., Nazarenko, L., Lacis, A., Schmidt, G. A., et al. (2005). Efficacy of climate forcings. *Journal of Geophysical Research*, *110*, D18104. https://doi.org/10.1029/2005JD005776

Jonsson, A. I., Fomichev, V. I., & Shepherd, T. G. (2009). The effect of nonlinearity in CO_2 heating rates on the attribution of stratospheric ozone and temperature changes. *Atmospheric Chemistry and Physics*, *9*(21), 8447–8452. https://doi.org/10.5194/acp-9-8447-2009

McLandress, C., Shepherd, T. G., Jonsson, A. I., von Clarmann, T., & Funke, B. (2015). A method for merging nadir-sounding climate records, with an application to the global-mean stratospheric temperature data sets from SSU and AMSU. *Atmospheric Chemistry and Physics*, *15*(16), 9271–9284. https://doi.org/10.5194/acp-15-9271-2015

Morgenstern, O., Hegglin, M. I., Rozanov, E., O'Connor, F. M., Abraham, N. L., Akiyoshi, H., et al. (2017). Review of the global models used within phase 1 of the Chemistry-Climate Model Initiative (CCMI). *Geoscientific Model Development*, *10*, 639–671. https://doi.org/10.5194/gmd-10-639-2017

Myhre, G., & Stordal, F. (1997). Role of spatial and temporal variations in the computation of radiative forcing and GWP. *Journal of Geophysical Research*, *102*(D10), 11,181–11,200. https://doi.org/10.1029/97JD00148

Myhre, G., Shindell, D., Breon, F.-M., Collins, W., Fuglestvedt, J., Huang, J., et al. (2013). Anthropogenic and natural radiative forcing. In *Climate change 2013: The physical science basis. Contribution of working group I to the Fifth Assessment Report of the Intergovernmental Panel on Climate Change 8* (pp. 659–740). Cambridge, United Kingdom and New York, NY, USA: Cambridge University Press. https://doi.org/10.1017/CBO9781107415324.018

Ramaswamy, V., & Bowen, M. M. (1994). Effect of changes in radiatively active species upon the lower stratospheric temperatures. *Journal of Geophysical Research*, *99*(D9), 18,909–18,921. https://doi.org/10.1029/94jd01310

Ramaswamy, V., Boucher, O., Haigh, J., Hauglustaine, D., Haywood, J., Myhre, G., et al. (2001). Radiative forcing of climate change. In *Climate change 2001: The physical science basis. Contribution of working group I to the Third Assessment Report of the Intergovernmental Panel on Climate Change 6* (pp. 349–417). Cambridge, United Kingdom and New York, NY, USA: Cambridge University Press.

Ramaswamy, V., Chanin, M.-L., Angell, J., Barnett, J., Gaffen, D., Gelman, M., et al. (2001). Stratospheric temperature trends: Observations and model simulations. *Reviews of Geophysics*, *39*(1), 71–122. https://doi.org/10.1029/1999rg000065

Rap, A., Richards, N. A. D., Forster, P. M., Monks, S. A., Arnold, S. R., & Chipperfield, M. P. (2015). Satellite constraint on the tropospheric ozone radiative effect. *Geophysical Research Letters*, *42*, 5074–5081. https://doi.org/10.1002/2015gl064037

Seidel, D. J., Gillett, N. P., Lanzante, J. R., Shine, K. P., & Thorne, P. W. (2011). Stratospheric temperature trends: Our evolving understanding. *Wiley Interdisciplinary Reviews: Climate Change*, *2*(4), 592–616. https://doi.org/10.1002/wcc.125

Sexton, D. M. H., Grubb, H., Shine, K. P., & Folland, C. K. (2003). Design and analysis of climate model experiments for the efficient estimation of anthropogenic signals. *Journal of Climate*, *16*(9), 1320–1336. https://doi.org/10.1175/1520-0442-16.9.1320

Shindell, D. T., Pechony, O., Voulgarakis, A., Faluvegi, G., Nazarenko, L., Lamarque, J.-F., et al. (2013). Interactive ozone and methane chemistry in GISS-E2 historical and future climate simulations. *Atmospheric Chemistry and Physics*, *13*(5), 2653–2689. https://doi.org/10.5194/acp-13-2653-2013

Shine, K. P., Bourqui, M. S., Forster, P. M. D. F., Hare, S. H. E., Langematz, U., Braesicke, P., et al. (2003). A comparison of model-simulated trends in stratospheric temperatures. *Quarterly Journal of the Royal Meteorological Society*, *129*, 1565–1588. https://doi.org/10.1256/qj.02.186

Søvde, O. A., Hoyle, C. R., Myhre, G., & Isaksen, I. S. A. (2011). The HNO_3 forming branch of the HO_2 + NO reaction: Pre-industrial-to-present trends in atmospheric species and radiative forcings. *Atmospheric Chemistry and Physics*, *11*(17), 8929–8943. https://doi.org/10.5194/acp-11-8929-2011

Søvde, O. A., Hoyle, C. R., Myhre, G., & Isaksen, I. S. A. (2012). Corrigendum to "the HNO_3 forming branch of the HO_2 + NO reaction: pre-industrial-to-present trends in atmospheric species and radiative forcings" published in Atmos. Chem. Phys., 11, 8929–8943, 2011. *Atmospheric Chemistry and Physics*, *12*(16), 7725–7725. https://doi.org/10.5194/acp-12-7725-2012

Stevenson, D. S., Young, P. J., Naik, V., Lamarque, J.-F., Shindell, D. T., Voulgarakis, A., et al. (2013). Tropospheric ozone changes, radiative forcing and attribution to emissions in the Atmospheric Chemistry and Climate Model Intercomparison Project (ACCMIP). *Atmospheric Chemistry & Physics*, *13*, 3063–3085. https://doi.org/10.5194/acp-13-3063-2013

Schwarzkopf, M. D., & Ramaswamy, V. (2008). Evolution of stratospheric temperature in the 20th century. *Geophysical Research Letters*, *35*, L03705. https://doi.org/10.1029/2007gl032489

van der A, R. J., Allaart, M. A. F., & Eskes, H. J. (2010). Multi sensor reanalysis of total ozone. *Atmospheric Chemistry and Physics*, *10*(22), 11,277–11,294. https://doi.org/10.5194/acp-10-11277-2010

Young, P. J., Archibald, A. T., Bowman, K. W., Lamarque, J.-F., Naik, V., Stevenson, D. S., et al. (2013). Pre-industrial to end 21st century projections of tropospheric ozone from the Atmospheric Chemistry and Climate Model Intercomparison Project (ACCMIP). *Atmospheric Chemistry & Physics*, *13*, 2063–2090. https://doi.org/10.5194/acp-13-2063-2013